Vietnam Journal of Catalysis and Adsorption
Tạp chí xúc tác và hấp phụ Việt Nam

http://chemeng.hust.edu.vn/jca/

Effect of carbonization temperature on the lithium storage performances of porous Sb/C nanocomposite

Le Thi Thu Hang*, Nguyen Thi Thu Huyen, Hoang Thi Bich Thuy

[1] *School of Chemical Engineering, Hanoi University of Science and Technology, Hanoi, VIETNAM*
**Email: hang.lethithu@hust.edu.vn*

ARTICLE INFO

Received: 20/2/2020
Accepted: 30/3/2020

Keywords:

Antimony, composite, lithium storage, cyclability.

ABSTRACT

In the present study, Sb/C nanocomposites have been synthesized using citrate-gel method in combination with a carbonization process at different temperatures in N_2 gas. At reasonable carbonization temperatures, the porous Sb/C nanocomposites with novel foam like-interconnected three-dimensional structure, which is built-up by nanosized Sb particles covered by a carbon shell, are obtained. Among the synthesized composites, the Sb/C-600 sample, which is calcinated at 600 ^oC, exhibit the best lithium storage. At a discharge-charge rate of 0.1 C, the Sb/C-600 electrode can supply an initial reversible specific capacity of 640.7 mA h g^{-1}, 1.7 times higher than the theoretical specific capacity of graphite anode. During 100 cycles, the electrode shows a slight capacity decay with 0.0348% of loss capacity per cycle. Because of this featured architecture, the Sb/C nanocomposites severe as anode material with enhanced lithium storage performances for rechargeable lithium ion batteries.

Introduction

Increasing energy demand becomes driving-force for scientists and engineers to investigate and develop outstanding-performance energy storage and conversion sources.[1] Nowadays, rechargeable lithium ion batteries (LIBs) have been used in diversity applications from household devices, transportation vehicles, medical equipment, to military equipment thanks to their superior properties to other batteries. Unfortunately, the state-of-art technology of this kind of rechargeable battery exhibits some issues, which stem from the intrinsic nature of both commercialized anode and cathode materials, and even from organic electrolytes.

Regarding the anode side, currently graphite has been utilized as anode material for most LIBs available on the global battery market. The reasons that this material is used popularly are its low cost, simple fabrication process, natural abundance, low working potential, high stability, environmental compatibility.[2] However, its disadvantages such as low theoretical capacity (372 mA h g^{-1}), exfoliation phenomenon during lithiation process and high safety risk at high discharge current rates due to formation of highly reactive dendritic Li metal (the working potential of graphite is closed to the deposition potential of Li metal) are still challenged.

Recently, alloying-type anode materials have been reported to have a potential of replacing graphite anode material in LIBs owing to their safer working potential (up to few hundreds of millivolts higher than Li^+/Li), and much higher specific capacity compared with graphite.[3] Among them, Sb-based materials have appeared as a suitable alternative due to their high theoretical lithium storage capacity (660 mA h g^{-1}) and

small volumetric change during lithiation process (~135%). Furthermore, compared with alloying type materials such as Si, Ge, or metal oxides or other metal sulfides, Sb is well-known to possess much higher conductivity.[4] This is also a desired property for any electrode active material. Despite its advantages, Sb, and other alloying-type anode materials as well, has been facing some scientific and technological challenges prior to commercialization. The most noticeable challenge is pulverization phenomenon of the electrode materials induced by volumetric expansion, accompanied by severe capacity fading.

So far, many efforts have been implemented to enhance the lithium storage capability and cycling stability for Sb-based materials, for example, fabrication of nanosized materials,[3] fabrication of composites with inactive/less active materials,[2,5] designs of novel structures.[6] In the previous report, we introduced a simple method to synthesize the porous Sb/C nanocomposites by using Sb(III)-citrate complex as precursor, followed by conventional carbonization in N_2 gas.[7] The obtained Sb/C composites exhibited remarkable electrochemical performances for LIBs application. The extraordinary properties were attributed to encapsulating Sb nanoparticles into interconnected carbon shell to form a novel three-dimensional (3D) structure. This suggests that carbonization stage surely plays an important role, influencing the microstructure of the obtained Sb/C composites, eventually their lithium storage capability.

In this study, the effect of the carbonization temperature on the lithium storage capability has been investigated. As expected, only at a optimal carbonization temperature of 600 ^oC the Sb/C composite exhibited highest lithium storage capability with a reversible specific capacity of 634.4 mA h g^{-1} at the 0.1C-rate of discharge-charge. This demonstrate that, to commercialize the Sb/C anode material for next generation LIBs, numerous parameters of its fabrication technology are needed to be optimized.

Experimental

Fabrication of Sb/C nanocomposites

Different Sb/C nanocomposites were prepared via citrate-gel method, followed by a thermal reduction at high temperature. In particular, 4.56 g of $SbCl_3$ (Sigma Aldrich, ≥99%) and 11.55 g of citric acid (sigma Aldrich, ≥99.5%) were added in 40 mL of an aqueous solution containing 2 M HCl. After being subjected to constant stirring for 10 min, a homogeneous solution of Sb(III)-citrate complex was produced. Next, this complex was heated at 100 ^oC to transform to a powdery type. Finally, the powder was calcinated in N_2 gas at three different temperatures of 550, 600 and 650 ^oC for 1 h. After cooling down to room temperature, the samples were taken out and labelled as Sb/C-550, Sb/C-600 and Sb/C-650, respectively.

Microstructure characterizations

Scanning electron microscopy (SEM) and transmission electron microscopy (TEM) were used to investigate the surface morphology and microstructure of the synthesized samples. The SEM analysis was carried out on SEM equipment with a S-4700 model while TEM analysis was performed on a TEM-EDX device system (model: Tecnai G2), which was equipped with Energy-dispersive X-ray spectroscopy (EDX). Crystalline structure and phase purity of the materials were also determined by using a X-ray powder diffractometer (XRD, model: D/MAX Ultima III).

Electrochemical characterization

In order to investigate lithium storage properties of the Sb/C nanocomposites, CR2032-type coin half cells were prepared. Firstly, a mixture including 40 mg of a Sb/C nanocomposite as electrode active material, 5 mg of carbon super P as conducting agent and 5 mg of lithium polyacrylate as binder was mixed well using an agate mortar and pestle. After that, an adequate amount of deionized water was added and mixed well again to form a homogeneous black slurry. This slurry was then casted on a copper foil as current collector using a doctor blade. After drying process at 100 ^oC for 6 h, the copper foil was punched into small dishes with a diameter of 14 mm, which were utilized as working electrodes in the coin cells. Subsequently, the cell assembly was proceeded in a argon gas filled-glove box. Each coin cell was constructed by a Sb/C composite electrode as working electrode, a circle Li foil as a counter/reference electrode and a Whatman® glass fiber piece as separator, which was soaked with 80 µL of 1M $LiPF_6$ and 5% fluoride ethylene carbonate (FEC) additive in a 50v/50v mixture of ethylene carbonate/dimethyl carbonate (EC/DMC) solvents.

The lithiation/delithiation mechanism of the Sb/C nanocomposites was investigated by using cyclic voltammetry (CV) measurement on a Gamry Potentiostat instrument. Lithium storage capability and stability were examined by galvanostatic charging-discharging (GCD) technique on an automatic battery

cycler (WonATech-WBCS 3000). The loading mass of the electrodes was controlled at 1.0 ± 0.1 mg cm^{-2}. The specific capacities were calculated according to the mass of the active material.

Results and discussion

Figure 1 presents the XRD patterns of the different Sb/C composites. In general, it can be seen that all diffraction peaks of the Sb/C composites reflected the presence of crystalline Sb phase with rhombohedral structure (JCPDS 01-085-1323). Noticeably, as for the Sb/C-550 composite, some tiny diffraction peaks of crystalline Sb_2O_3 phase with typical cubic structure (JCPDS 01-072-1334) was recorded. This demonstrates that Sb/C-550 composite contained a small impurity phase. In addition, no characteristic diffraction peaks of crystalline C phase were detected, suggestion amorphous nature of C present in all samples of Sb/C composite.

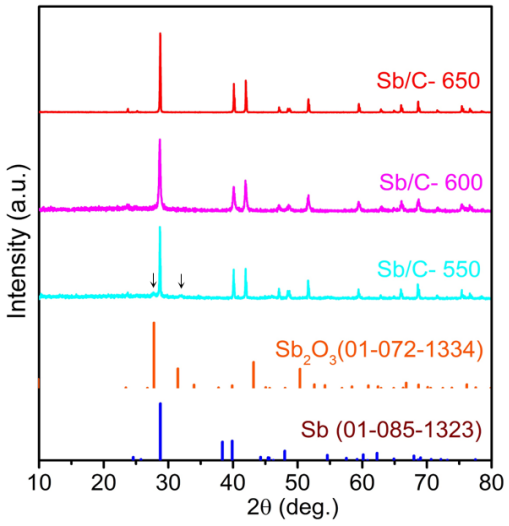

Figure 1: XRD patterns of Sb/C composites synthesized at different temperatures.

Based on the obtained XRD analysis results, it is stated that during calcination process in N_2 gas atmosphere, the carbonization and thermal reduction occurred simultaneously. From Sb(III)-citrate complex as Sb and C sources, Sb_2O_3, Sb, C were formed according to the following reactions:[8]

$$2Sb(C_6H_5O_7)_2 \rightarrow Sb_2O_3 + C + 10H_2O + 7CO_2 + CO \quad (1)$$

$$Sb_2O_3 + 3CO \rightarrow 2Sb + 3CO_2 \quad (2)$$

$$CO_2 + C \rightarrow 2CO \quad (3)$$

As reported in the literature,[9] the reduction of Sb_2O_3 by carbon often started at temperatures of 502–596 °C. In the present work, the calcination temperatures selected for investigation 550, 600 and 650 °C. The calcination temperature higher than 650 °C were not investigated. The reason is because the melting point of Sb_2O_3 is 655 °C.[10] This probably causes the precursor loss of Sb. Obviously, according to the routine of fabricating Sb/C in this study, at 550 °C, the thermal reduction of Sb_2O_3 to produce Sb occurred incompletely. Thus, impurity phase of Sb_2O_3 with very weak diffraction intensity was detected.

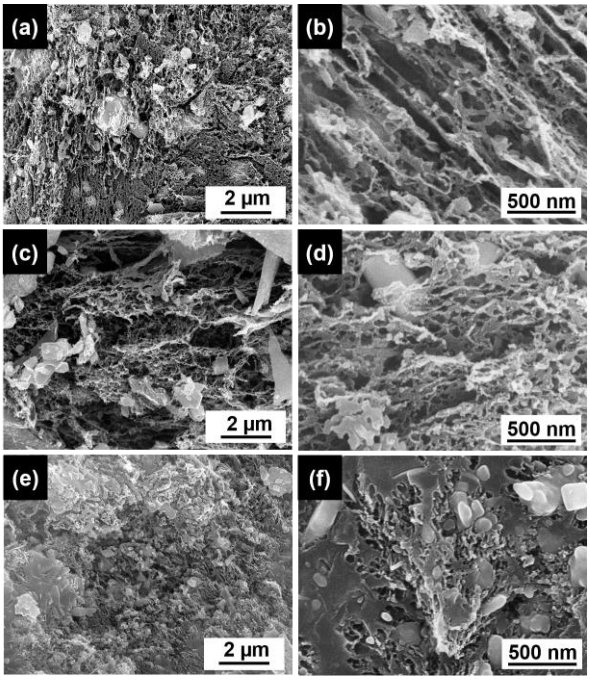

Figure 2: SEM images with low and high magnifications of Sb/C composites: (a,b) Sb/C-550, (c,d) Sb/C-600, (e,f)Sb/C-650.

Figure 2 shows SEM images of the Sb/C composites calcinated at different temperatures. As observed from the SEM images with low magnification (Figs. 2a,c,e), the Sb/C composites seem to possess 3D foam-like highly porous structure, which is often regarded as favorable structure for rapid Li^+ diffusion in working LIBs.[11] The nanoporous structure of the Sb/C composites were recognized more clearly in the SEM images with high magnification (Figs. 2b,d,f). Plenty of pores formed between interconnected Sb/C particles. The presence of the pores resulted from gas evolution induced by the decomposition of citric acid during the calcination process to prepare the composites (Eq.1 - Eq.3). Interestingly, as for the Sb/C-650 composite (Figure 2f), its structure appears less porous than those calcinated at lower temperatures. Herein, the aggregation phenomenon of Sb particles in the Sb/C-650 composite observed after calcination is probably due to relatively low melting point of Sb (631 °C).[12] Despite being already formed during the

calcination process, the C shell seems to impossibly isolate completely Sb particles. As a result, the high porosity was no longer observed for the Sb/C-650 composite.

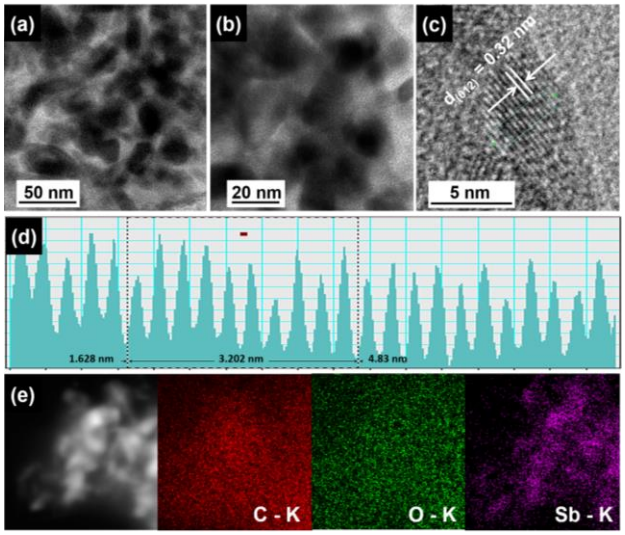

Figure 3: (a-c) TEM images of Sb/C-600 composite; (d) d-spacing of Sb present in Sb/C-600; (e) EDX elemental mapping of Sb/C-600 composite.

To further verify the nanoporous structure of the synthesized composites, the internal structure of the typical Sb/C-600 composite was examined using TEM method. As shown in Figs. 3a,b, the black particles of 10-50 nm size were covered by a outside greyish layer. The high dense cores represent Sb nanoparticles while the outer low dense layer characterizes the C shell. This core-shell structure was identified clearly in Figure 3c, the high resolution TEM image of Sb/C-600 composite. Herein, the presence of a Sb nanocrystal with (012) orientation was confirmed by d-spacing of ~0.32 nm (as result measured in Figure 3d). Meanwhile, the presence of the outer C shell was recognized by a low dense layer composed of C atoms which were not organized in long-range order.

The uniform distribution of Sb as main electrode active material in the C framework is an important factor which strongly impacts the lithium storage behavior of the resultant nanocomposites. Thereby, EDS elemental maps of the composites including C, O, and Sb were recorded. As a feature sample, the Sb/C-600 exhibited uniform distribution of C and Sb elements over the entire measured sample. This proved that Sb nanoparticles were completely covered by the C layer. The complete covering of the C layer ensured the good electrical contact among the Sb active material particles.[13] Remarkably, the presence of O element was still detected although the sample was deaerated under high vaccum condition prior to TEM-EDS measurement, and the Sb_2O_3 phase in the Sb/C-600 composite was no longer detected by XRD. According to the previous report, [7] the presence of O element in the Sb/C-600 sample possibly results from its highly porous structure, which easily adsorbed oxygen from the air on the surface of the material. Thus, the signal of O element can be regarded as the trace of O_2 adsorbed on the surface of Sb/C-600. Furthermore, after the carbonization process, the remaining C materials normally possess the surface functionalized by groups such as C-O, C=O, C-OH. As a result, the O element was frequently detected for the synthesized cabonaceous materials.[2,13] This indicated that, in the present work, the surface of C present in the Sb/C-600 composite was functionalized during the synthesis process.

In order to investigate Li lithiation/delithiation mechanism, the Sb/C-600 electrode was examined by CV method. In particular, the electrode was cycled at the potential between 0.01 and 1.5 V *vs.* Li^+/Li with a scan rate of 0.1 mV s^{-1}. Figure 5a displays the CV plots of the Sb/C-600 electrode for five cycles with open circuit potential (OCP) as a starting point of recording process. In the first cycle, the Sb/C-600 possessed two cathodic peaks. A peak was located at 0.78 V and the another was centered at 0.51 V *vs.* Li^+/Li. They are characteristic of an irreversible formation of a solid electrolyte interface (SEI) layer on the electrode surface and lithiation of Sb to form the Li_3Sb alloy, respectively. Besides, the increase in cathodic current at the potential reaching 0.01 V *vs.* Li^+/Li was also observed. According to the previous report,[14,15] this phenomenon is related to the underpotential deposition of Li metal into C framework present the Sb/C composite. In the anodic scan, only a sharp oxidation peak was found at 1.09 V *vs.* Li^+/Li. This corresponds to the delithiation of Li_xSb to produce Sb. From the second cycle onwards, as for both cathodic and anodic scans only a reduction (or oxidation) peak was recorded, implying the formation of the SEI layer only happened at the first cycle. It is also noticed that the third-to-fifth CV plots almost coincided with the second CV plot, demonstrating the stability of the formed SEI layer as well as the high reversibility of Sb/C-600 composite.

Figures. 4b-d illustrate the discharge-charge voltage profiles of the Sb/C composite electrodes. On the whole, at the first discharge, all the electrodes exhibited a rapid decrease potential from OCP to the potential of

~ 0.75 V, corresponding to the irreversible formation of the SEI layer. After that, the cell potential almost remained at 0.5 V before quickly dropping to a lower cut-off voltage of 0.01 V. This step corresponds the Li insertion into the composites. For subsequently reversible process, the composite electrodes only had a charge plateau at around 1.1 V, which was associated

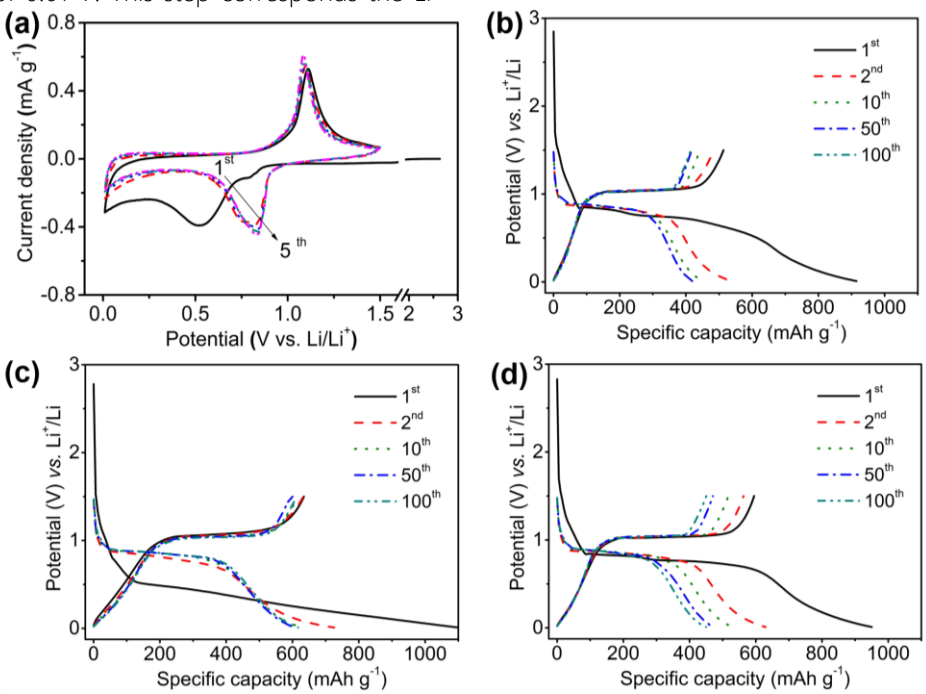

Figure 4: Electrochemical properties of Sb/C composites: (a) CV plots of Sb/C-600 electrode for initial cycles at a scan rate of 0.1 mV s^{-1}, Discharge-charge voltage profiles of (b) Sb/C-550, (c) Sb/C-600 and (d)-Sb/C-650 electrodes at the 0.1C rate for 100 cycles of discharge-charge.

to their Li extraction. These obtained results are in accordance with the CV result in Figure 4a. From the second cycle onwards, the discharge-charge profile of the composite electrodes hardly changed, especially for the Sb/C-600 electrode, suggesting its high stability during cell operation.

At the first cycle, the Sb/C-550, Sb/C-600 and Sb/C-650 electrode delivered the discharge/charge specific capacities of 915.3/513.3, 1110.6/640.7, and 950.4/594.9 mA h g^{-1}, respectively. Accordingly, their initial coulombic efficiency (CE) was found to be relatively low, viz. 56.1% for Sb/C-550, 57.7% for Sb/C-600, and 62.6% for Sb/C-650. The higher CE of the Sb/C-650 was attributed to the lower porosity in comparison with the rest other composites (Figure 2). According to Zhou and co-workers' report, a low initial CE is a popular phenomenon for carbonaceous materials prepared at the low temperature (500-700 °C).[16] Thereby, the CE can be improved by enhancing the carbonization temperature. Unfortunately, in this study, it is difficult to elevate the carbonization temperature further because of the limit of the melting point of Sb and Sb_2O_3. This will be clarified by lithium storage behavior of the resultant Sb/C composites in the following discussion.

Figure 5 presents the cycle number-dependence of the reversible specific capacity of the Sb/C composites and their relevant CEs for 100 cycles at a discharge-charge rate of 0.1C. As shown in Figure 5a, the specific capacity of the electrodes degraded in the first five cycles. This probably was attributed to the structural collapse of porous C present in the Sb/C during delithiation. However, this process only occurred at the edge of C framework, which can contain chemically active sites or the surface functional groups (C-O, C=O,...).[7] Then, the microstructure of the composites stabilized gradually in the following cycles. Among three electrodes, the Sb/C-600 exhibited the highest specific capacity and the most stable capacity retention. At the fifth cycle, the Sb/C-600 electrode offered a reversible specific capacity of 605.1 mA h g^{-1}. Meanwhile, the Sb/C-550 and Sb/C-650 electrodes only delivered 458.8 and 531.2 mA h g^{-1}, respectively. After 100 cycling test, the Sb/C-600 electrode still achieved a reversible specific capacity of 593 mA h g^{-1}, corresponding to 98% capacity retention of the initial capacity. In contrast, the Sb/C-550 and Sb/C-650 had only 90.3% and 84.8% capacity retention. Herein, during cycling test, the capacity of the electrodes was arranged in the order: Sb/C-600 > Sb/C-650 > Sb/C-

550. This can be explained that although the Sb/C-650 and Sb/C-600 only contained pure Sb without any Sb_2O_3 phase, the Sb/C-650 composite had lower porosity than Sb/C-600. This leads to the lower capacity of Sb/C-650. Meanwhile, among three composite samples, solely the Sb/C-550 contained Sb_2O_3 impurity phase, which was reported to have a lower lithium storage capability than that of Sb.[17] As a result, the lithium storage capability of Sb/C-550 was inferior.

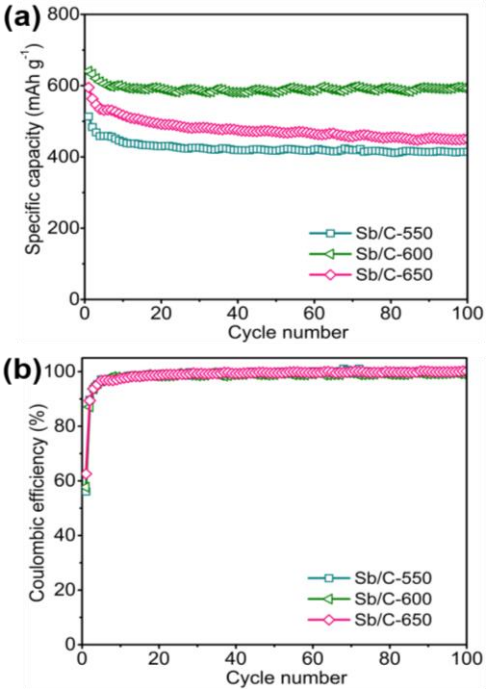

Figure 5: Cycability and corresponding coulombic efficiency of the different Sb/C composite electrodes at 0.1C-rate for 100 cycles.

The corresponding CEs of the Sb/C electrodes at the 0.1C-rate are present in Figure 5b. Excluding the low CE values for first ten cycles, at the subsequent cycles of discharge-charge, all the Sb/C electrodes attained very high CEs, fluctuating between 97.5% and 99.9%. This is accounted for the utilization of FEC additive in the electrolyte, which stabilized the SEI layers of the electrodes, and the small volume change of Sb during the cycling process.

Conclusion

The effect of the calcination temperature (within a temperature range of 550-650 °C) on the lithium storage behaviors of the Sb/C nanocomposites was investigated. The Sb/C nanocomposites were fabricated via citrate-gel method and followed by calcination in an inert gas. The XRD, SEM, TEM and EDS mapping results demonstrated that the synthesized Sb/C nanocomposites possessed the novel core-shell structure, where Sb nanoparticles as cores were covered by an outer carbon layer as shell, and the Sb nanoparticles were interconnected together to build up a foam-like 3D architecture. Accordingly, the Sb/C composites exhibited excellent lithium storage behavior in term of high specific capacity and stable cyclability. Among the composites, the sample was calcinated at 600 °C was proved to have highest capacity of 640.7 mAh g^{-1}, which was more than 1.7 times as high as the theoretical capacity of commercial graphite anode, demonstrating high application potential for advanced LIBs.

Acknowledgments

This research is funded by Vietnam National Foundation for Science and Technology Development (NAFOSTED) under grant number 104.99-2017.305. We also gratefully acknowledge Professor Chan-Jin Park for use of his equipment in Materials Electrochemistry Laboratory at Chonnam National University (South Korea).

References

1. G.E. Blomgren, J. Electrochem. Soc., 164 (2016) A5019.
2. X. Liu, Y. Tian, X. Cao, X. Li, Z. Le, D. Zhang, X. Li, P. Nie, H. Li, ACS Appl. Energy Mater., 1 (2018) 6381-6387.
3. Z. Chen, Y. Cao, J. Qian, X. Ai, H. Yang, J. Mater. Chem., 20 (2010) 7266-7271.
4. J. He, Y. Wei, T. Zhai, H. Li, Mater. Chem. Front., 2 (2018) 437-455.
5. F.-S. Ke, L. Huang, B.C. Solomon, G.-Z. Wei, L.-J. Xue, B. Zhang, J.-T. Li, X.-D. Zhou, S.-G. Sun, J. Mater. Chem., 22 (2012) 17511-17517.
6. H. Kim, J. Cho, Chem. Mater., 20 (2008) 1679-1681.
7. H.T.T. Le, X.-M. Pham, C.-J. Park, New Journal of Chemistry, 43 (2019) 10716-10725.
8. T. Gutknecht, C. Forsgren, B.-M. Steenari, J. Clean. Prod., 162 (2017) 474-483.
9. T. Karlsson, C. Forsgren, B.-M. Steenari, J. Sustain. Met., 4 (2018) 194-204.
10. R.G. Orman, D. Holland, J. Solid State Chem., 180 (2007) 2587-2596.

11. J. Su, H. Liang, X.-N. Gong, X.-Y. Lv, Y.-F. Long, Y.-X. Wen, Nanomaterials (Basel), 7 (2017) 121.

12. Y. Zhu, X. Han, Y. Xu, Y. Liu, S. Zheng, K. Xu, L. Hu, C. Wang, ACS Nano, 7 (2013) 6378-6386.

13. X.-M. Pham, D.T. Ngo, H.T.T. Le, P.N. Didwal, R. Verma, C.-W. Min, C.-N. Park, C.-J. Park, Nanoscale, 10 (2018) 19399-19408.

14. H.T.T. Le, T.-D. Dang, N.T.H. Chu, C.-J. Park, Electrochim. Acta, 332 (2020) 135399.

15. J.R. Dahn, T. Zheng, Y. Liu, J.S. Xue, Science, 270 (1995) 590.

16. H. Zhou, S. Zhu, M. Hibino, I. Honma, M. Ichihara, Adv. Mater., 15 (2003) 2107-2111.

17. M.-Z. Xue, Z.-W. Fu, Electrochem. commun., 8 (2006) 1250-1256.